C. R. Chimie 18 (2015) 283–292

Contents lists available at ScienceDirect

Comptes Rendus Chimie

www.sciencedirect.com

GeCat 2014: Advances and prospects in heterogeneous catalysis

Optimization of structured cellular foam-based catalysts for low-temperature carbon dioxide methanation in a platelet milli-reactor

Myriam Frey [a], David Édouard [b,c], Anne-Cécile Roger [a,*]

[a] ICPEES, UMR 7515, UMR 7515, Group "Energy and Fuels for a Sustainable Development", 25, rue Becquerel, 67087 Strasbourg, France
[b] University of Strasbourg Institute for Advanced Study (USIAS), 67000 Strasbourg, France
[c] Laboratoire d'automatique et de génie des procédés (LAGEP), Université Claude-Bernard Lyon-1, UMR CNRS 5007, 43, boulevard du 11-Novembre-1918, 69622 Villeurbanne, France

ARTICLE INFO

Article history:
Received 30 June 2014
Accepted after revision 6 January 2015
Available online 7 February 2015

Keywords:
Structured milli-reactors
Foam
Carbon nanofibers
CO_2 hydrogenation
Methanation
Ceria–zirconia

ABSTRACT

Here, we present a preliminary study to choose a catalyst with enough catalytic activity at temperatures below 250 °C, in order to study heat transfer in a platelet milli-reactor (PMR) with an infrared camera and a commercial window inserted on the top of our reactor that only withstands a maximal temperature of 250 °C. The higher methane productivity of foam catalysts compared to powder catalysts was revealed. Foam catalysts, all impregnated with the same amount of active phase (Ni + Ru) and with different coatings, were compared to SiC only impregnated with Ni + Ru. The different coatings studied were: carbon nanofibers (CNF), ceria–zirconia (CZ) and the combination of both. Both CNF and CZ washcoats were able to increase the low specific surface area of the SiC foam. Moreover, the presence of ceria–zirconia was proven to be essential for ensuring high methane productivities. The catalyst combining both CNF and CZ showed the best results.

1. Introduction

Carbon dioxide has always been present in the atmosphere in small quantities. There are natural sources responsible for its presence (breathing, fermentation, fires, volcanoes, decomposition of organic matter…), but also anthropogenic ones (combustion of fossil sources and biomass, industries, agriculture…), the contribution of which being massively and constantly increasing since the beginning of the industrial revolution. Carbon dioxide is one of the gases responsible for the greenhouse effect. In order to reduce the CO_2 production or its emission into the atmosphere, a lot of research projects about capture and storage emerged [1].

Another pathway to reduce these emissions is the valorisation of CO_2 by transformation into valuable chemical compounds, like methane or longer hydrocarbon species, methanol, esters, ethers… [2].

The production of methane using CO_2 as a reactant is therefore a suitable way to contribute to the decrease of greenhouse gas emissions through chemical recycling. Using conventional electricity, made for example from fossil fuel, would be nonsense, contrary to the power-to-gas concept where the excess of energy mainly produced by wind parks or solar-electric generation is used. The hydrogen necessary for the methanation reaction is produced by water electrolysis and reacts with carbon dioxide to produce methane that can be directly injected into the natural gas grid. Few projects are already at the state of demonstration project, for example the ENERTAG

* Corresponding author.
E-mail addresses: myriam.frey@etu.unistra.fr (M. Frey), david.edouard@univ-lyon1.fr (D. Édouard), annececile.roger@unistra.fr (A.-C. Roger).

http://dx.doi.org/10.1016/j.crci.2015.01.002
1631-0748/

project (2011) [3], which uses excess energy from wind parks to produce hydrogen combined with a biogas plant to produce biomethane, or Audi (2013) [4] with a power-to-gas facility of 6 MW to produce methane for their new gas powered cars.

The methanation reaction was discovered by Sabatier and Senderens in 1902 [5,6], who studied the hydrogenation reaction of CO and CO_2 on nickel or cobalt. Since then many studies on metallic elements of group VIII (Fe [7], Rh [8,9], Ru [10,11], Co [12] or Ni [9,13–19]) supported on oxides (TiO_2, CeO_2, ZrO_2, Al_2O_3, SiO_2, La_2O_3, La_2O_3/SiC [18]...) or mixed oxides [9,18–21] were published.

During the hydrogenation of carbon dioxide into methane (1), other side products like alkanes (2), alkenes (3), and CO through Reverse Water Gas Shift reaction (4) can be formed:

$$CO_2 + 4H_2 = CH_4 + 2H_2O \quad (1)$$

$$n\ \ CO_2 + (3n+1)H_2 = C_nH_{2n+2} + 2nH_2O \quad (2)$$

$$nCO_2 + (3n)H_2 = C_nH_{2n} + 2nH_2O \quad (3)$$

$$CO_2 + H_2 = CO + 2H_2O \quad (4)$$

Most of the studies that can be found in the literature about this reaction were done using powder catalysts in a fixed-bed reactor. The use of cellular foam instead of powder in a fixed-bed has many advantages such as a high surface/volume ratio, low pressure drop, a better control of the reaction conditions and an intensification of mass and heat transfer [22–24]. The last one is very interesting for the intensification of the methanation reaction. Effectively, the exothermicity of this reaction is partly responsible for the catalyst deactivation by enhancing the sintering of metallic particles.

The cellular foams used in this work, made of β-SiC and provided by SICAT [25], are synthesized using a shape memory synthesis developed by Ledoux et al. [26]. The use of β-SiC foams have some advantages: SiC is chemically inert, has a good mechanical and thermal resistance and presents a high thermal conductivity for a ceramic matrix. β-SiC shows however one major disadvantage, its low specific surface area (approx. 20 $m^2 \cdot g^{-1}$) which is due to its method of preparation that requires high temperatures. However, Édouard et al. [27] reported that by growing nanofibers on the foam's surface, the specific surface area can be increased up to 50 $m^2 \cdot g^{-1}$.

A new kind of platelet milli-reactor (PMR), shown on Fig. 1, has been developed by our institute for the intensification of catalytic processes like the dehydration of methanol into dimethylether [28,29], the oxidative dehydrogenation of ethane and ammoxidation of propane [30] and the Fischer–Tropsch synthesis [31]. But, up to date, no industrial processes have been reported using microreactors or PMR despite their advantages compared to conventional reactor. The PMR used in this study is composed of a metallic host structure where a cellular β-SiC foam with or without carbon nanofibers (CNF), impregnated with a catalyst, is inserted into a central channel (18 mm × 5 mm × 24 mm), as shown in Fig. 1. This PMR is used in order to enhance the methanation reaction

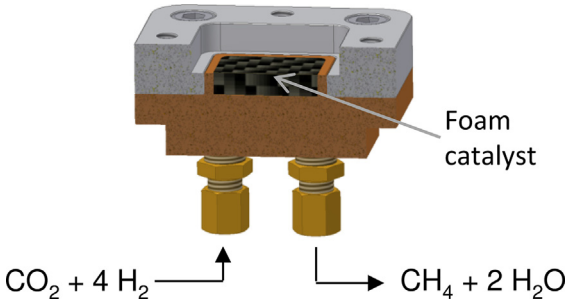

Fig. 1. (Color online.) Drawing of the platelet milli-reactor (PMR) developed for this study with a single central channel of 18 × 5 × 24 mm.

by combining the advantages of milli-reactors and β-SiC foam support.

The final objective of our work is to study the heat transfer of the highly exothermal carbon dioxide methanation reaction. In order to study the heat transfer, an infrared camera will be used and a commercial window inserted on the top of the PMR. The window used only stands a maximal temperature of 250 °C. Therefore, in this paper, we will present the preliminary studies made to choose a catalyst with enough catalytic activity at temperatures below 250 °C (10–20%). First, catalytic tests in a fixed-bed were made on powder catalyst, then on fragments of impregnated β-SiC foam, in order to choose which active phase will be deposited on the foams that will be tested in the PMR.

Nickel-based catalysts were chosen because they are efficient for CO_2 methanation in term of activity and selectivity [9,21], and are less expensive than ruthenium-based catalysts also used for methanation. A ceria–zirconia support, that has already been studied by our institute [32,33] and proven to show high conversion rates, methane selectivity and stability, was employed. Two powder catalysts impregnated with 10 w% of Ni and 0.1 wt% of Ru were compared: CZ_p (CZ being $Ce_2Zr_2O_8$) and SiC'_p. Six SiC foam-based catalysts (cell size 2700 μm, strut size 226 μm, window diameter 1146 μm, porosity 0.9), whose detailed compositions are summarized in Table 1, were also studied. The first one, SiC'_f, was a SiC foam impregnated with 10 w% of Ni and 0.1 wt% of Ru and was compared to SiC'_p catalyst to investigate the difference between foam and powder catalysts regarding the catalytic activity. The second one, $27CZ_f$, was a SiC foam with 27 wt% loading of ceria–zirconia and 2.5 wt% of Ni and 0.025wt% of Ru to have the same Ni/CZ ratio (1/9) than powder catalyst CZ_p. It will allow us to investigate the difference between foam and powder catalysts regarding the catalytic activity in the case of ceria–zirconia-based catalysts. The amount of active phase was set to 2.5 wt% of Ni and 0.025 wt% of Ru, to compare the foam catalysts studied. The third catalyst studied, SiC_f, was a SiC foam only loaded with the Ni and Ru active phases. The fourth catalyst studied, $15CNF_f$, was a SiC foam with 15 wt% loading of carbon nanofibers to study the influence of those CNF on the catalyst's activity. A SiC foam with 1 wt% of CZ was also synthesized, $1CZ_f$, to compare the effect of CNF and a ceria–zirconia-based catalyst with lower CZ content.

Table 1
(Color online.) Theoretical composition of the catalysts studied in this paper.

Catalysts		wt% SiC	wt% CZ	wt% CNF	wt% Ni	wt% Ru
◆	SiC'_p	89.9	–	–	10	0.1
■	CZ_p	–	89.9	–	10	0.1
△	SiC'_f	89.9	–	–	10	0.1
▲	SiC_f	97.5	–	–	2.5	0.025
×	$15CNF_f$	82.5	–	15	2.5	0.025
+	$1CZ_f$	96.5	1	–	2.5	0.025
✖	$27CZ_f$	82.5	–	27	2.5	0.025
□	$1CZ/15CNF_f$	81.5	1	15	2.5	0.025

CZ: ceria–zirconia; CNF: carbon nanofibers.

Finally, $1CZ/15NFC_f$; loaded with 15 wt% of CNF covered with 1 wt% of CZ, was synthesized to investigate the combined influence of CNF and ceria–zirconia.

2. Experimental

2.1. Catalyst preparation

2.1.1. Synthesis of $Ce_2Zr_2O_8$

$Ce_2Zr_2O_8$ was synthesized using a "pseudo sol–gel" method. The starting salts, cerium acetate (III) and zirconium acetylacetonate (IV), were dissolved separately in propionic acid (100 °C), in order to obtain a solution of 0.12 mol·L^{-1} and generate the desired metallic propionates. Both solutions were then mixed and heated under reflux for 2 h in order to give mixed propionates. A distillation under progressive vacuum is made to evaporate the solvent and leads, through oligomerization, to the formation of a resin. Finally, this resin was calcined for 6 h at 500 °C in the air.

2.1.2. Powder catalyst impregnation of Ni + Ru

An amount of 10 wt% of Ni^0 and 0.1 wt% of Ru^0 were loaded over these supports using the incipient wetness impregnation method with nickel nitrate hexahydrate and ruthenium acetylacetonate dissolved in ethanol. The catalyst was then dried at 100 °C for 2 h and calcined at 500 °C for 6 h in the air (heating rate 2 °C min^{-1}).

2.1.3. β-SiC pre-treatment

The β-SiC foams were first calcined at 900 °C for 2 h in the air in order to generate a natural SiO_2–SiO_xC_y washcoat layer [27] allowing a better anchoring of the active phase.

2.1.4. CNF synthesis

The cellular foams were impregnated with 3 wt% of Ni^0 using an ethanolic solution of $Ni(NO_3)_2{\cdot}6H_2O$, dried at 100 °C for 2 h and calcined at 350 °C in the air for 2 h (heating rate 2 °C min^{-1}). The synthesis of CNF was performed in a quartz tubular reactor (inner diameter 30 mm, length 600 mm). The sample was first reduced under a hydrogen flow (100 mL·min^{-1}) for 1 h at 400 °C (heating rate 3.5 °C min^{-1}). The temperature was increased to 680 °C (heating rate 3.5 °C min^{-1}) and the gas flow changed to the reaction mixture H_2/ethane (50 mL·min^{-1} and 100 mL·min^{-1}) for 2 h to generate the CNF. The temperature was then returned to ambient under argon. Finally, the samples were sonicated for 15 min to eliminate the CNF that are not well anchored.

2.1.5. Ceria–zirconia coating

The samples coated with ceria–zirconia, were dipped into a saturated propionic acid solution of pseudo sol-gel (cationic concentration of 0.94 M), dried overnight at 100 °C, and calcined for 6 h at 500 °C in the air. This step was repeated four times in order to have 30 wt% of CZ on the foam. A solution of 0.094 M and one dipping step was necessary to have 1 wt% of CZ on the SiC foam and SiC foam covered with carbon nanofibers.

2.1.6. Foam impregnation with Ni + Ru

The samples were impregnated with 2.5 wt% of Ni^0 and 0.025 wt% of Ru^0 by dipping them into an ethanolic solution of nickel nitrate hexahydrate and ruthenium acetylacetonate, and then dried at 100 °C for 2 h. The samples without CNF were calcined at 500 °C for 6 h in the air and the sample with CNF were first calcined at 200 °C for 2 h in the air, and after that, at 500 °C for 6 h under Ar.

2.2. Characterization

The specific surface area (SSA), average pore size and diameter of the different catalysts were determined by the Brunauer–Emmet–Teller (BET) method using N_2 adsorption–desorption measurements at 77 K (Micromeritics ASAP 2420). Prior to N_2 adsorption, the sample was outgassed at 250 °C for 3 hours to desorb moisture adsorbed on the surface and inside the porous network.

Scanning electron microscopy (SEM) micrographs were only used on the fragments to measure the diameter of CNF and to investigate the homogeneity of the CNF network and coating on the foam surface. SEM micrographs were taken with a JEOL FEG 6700F microscope.

Thermogravimetric analysis (TGA) experiments were performed from ambient to 1000 °C (heating rate 10 °C min^{-1}) in the air on the SiC foam to quantify the CNF synthesized.

X-ray diffraction patterns (XRD) were recorded on a Bruker D8 Advance diffractometer with a LynxEye detector and Ni filtered Cu Kα radiation (1.5418 Å) over a 2θ range of 25–100° and a position-sensitive detector using a step size of 0.012° and a step time of 0.5 s. The crystallite size of the samples was evaluated from X-ray broadening by using the Debye–Scherrer equation [34].

Hydrogen temperature-programmed reduction (H_2-TPR) on the powder samples was performed to evaluate the reducibility of the catalyst using a Micromeretics AutoChem II. TPR measurements were carried out on 100–150 mg of catalyst, loaded in a quartz U-tube and heated from room temperature to 900 °C (15 °C min^{-1}) under a flow of 10% H_2/Ar (50 mL·min^{-1}).

2.3. Catalytic test

The powder catalysts were sieved to use only the 125–200-μm fraction. The foam catalysts were fragmented and shaped to a cylinder with the same diameter than the reactor and a height of 5.5 mm. Carbon dioxide hydrogenation into methane was carried out under atmospheric pressure in a fixed-bed tubular reactor made of quartz (inner diameter 6.8 mm). The reaction temperature was monitored by using a thermocouple located inside the reactor. The Gas Hourly Space Velocity (GHSV) was set to 10,000 h^{-1} and the formula used was: $GHSV = \frac{Q}{V}$, Q is the flow rate (L·h^{-1}), and V is the apparent volume of the catalytic bed (L).

The gas flow rate was set to 25 mL·min^{-1}. For powders, the mass of catalyst was adjusted depending on its apparent density. The V value taken for the foam fragments was directly determined by calculating the volume taken (foam and volume taken by the empty cells) by the cylindrical fragment inserted into the quartz reactor.

The catalyst was pre-reduced in an 80:20 H_2:N_2 stream (46 mL·min^{-1}) at 400 °C (heating rate: 2 °C min^{-1}) for 6 h. The reactivity of the catalyst was followed at different temperatures: 150, 200, 250, 300, 350 and 400 °C (heating rate: 2 °C min^{-1}) under a stoichiometric flow of reactants: H_2/CO_2 (4:1), and N_2 as an internal standard. The molar ratio of H_2:CO_2:N_2 was 36:9:10, with a flow rate of 25 mL·min^{-1}. The feed and products were analyzed at every temperature using a programmable micro-chromatograph (Agilent M200H, TCD detector, alumina poraplot and molecular sieve 5-Å columns). The CO_2 conversion and CH_4 selectivity were defined as follows:

$$X_{CO_2}(\%) = \left(1 - \frac{A_{CO_2}}{A_{CO_2} + A_{CH_4} + A_{CO} + 2A_{C_2H_6}}\right) \times 100$$

$$S_{CH_4}(\%) = \left(\frac{A_{CH_4}}{A_{CO_2} + A_{CH_4} + A_{CO} + 2A_{C_2H_6}}\right) \times 100$$

X is the conversion, S the selectivity, and A the surface areas of the peaks obtained by chromatography and corrected by their corresponding gas response factors. The liquid phase was analyzed at the end of the reaction with a gas chromatograph (Agilent 6890N, SolGelWax column).

The methane productivity was also determined and defined as the amount of CH_4 moles produced per hour per gram of active phase (Ni + Ru).

3. Results and discussion

3.1. Characterization

All the catalysts (Fig. 2) show a set of reflections at 37°, 43° et 63°C, assigned to NiO (NiO, JCPD card No. 01-089-7131), except $15CNF_f$ that has reflections at 44° and 52°, assigned to Ni^0, due to the calcinations step under Ar. The reflections assigned to nickel crystallites are naturally less intense for the foams due to the smaller amount of nickel present. RuO_2 is not detected by XRD, because of the amount of metal present on the catalysts being under the detection limit of the apparatus.

The XRD patterns (Fig. 2) of CZ_p show the presence of the fluorite cubic structure ($Ce_{0.4}Zr_{0.6}O_2$, JCPD card No. 00-038-1439), usually observed for ceria–zirconia mixed oxide with high contents of ceria [35,36]. Reflections corresponding to (111), (200), (220), (311), (222) and (400) planes are observed. Furthermore, no CeO_2 or ZrO_2 segregation phases are detected. This indicates that zirconia is completely incorporated into the ceria lattice, forming a homogeneous solid solution. The X-ray powder diffractograms of SiC'_p, SiC_f and SiC'_f (diffractograms of foams not presented because it is similar to SiC'_p) also show the presence of a fluorite cubic structure corresponding to β-SiC (β-SiC, JCPD card No. 00-001-1119). Reflections corresponding to (111), (200), (220), (311), (222) and (400) planes are observed. The natural SiO washcoat cannot be seen by XRD.

The XRD pattern of $1CZ_f$ also shows that ceria–zirconia and SiC have both a fluorite cubic structure, but the peaks are broader and seem to be split, which indicates the

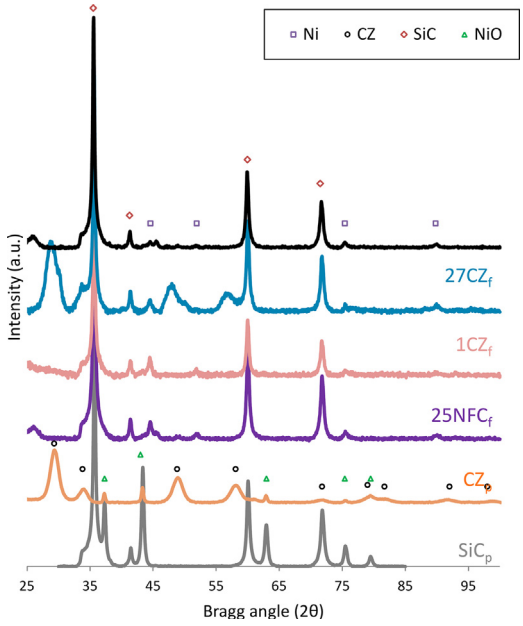

Fig. 2. (Color online.) Powder diffractogram of the catalysts studied.

Table 2
XRD results: crystallite size (D) calculated with the following reflections: (220), (400), (422) and (333), and cubic lattice parameter (a); BET results: mesoporous diameters (D_{pores}), mesoporous volumes (V_{pores}), and specific surface area (SSA).

Catalyst		XRD						BET		
		D_{SiC} (nm)	D_{CZ} (nm)	D_{NiO} (nm)	D_{RuO2} (nm)	a_{SiC} (Å)	a_{CZ} (Å)	D_{pores} (nm)	V_{pores} (cm^3/g)	SSA (m^2/g)
⬚	SiC'_p	31.2	–	24.9	nd	4.352	–	17.8	0.13	6
✖	CZ_p	–	7.1	33.5	nd	–	5.268	4.4	0.05	31
△	SiC'_f	31.2	–	24.9	nd	4.352	–	17.3	0.19	10
▲	SiC_f	31.4	–	18.6	–	4.357	–	15.2	0.12	25
×	$15CNF_f$	27.6	nd	18.1	nd	4.356	nd	12.2	0.15	40
+	$1CZ_f$	31.2	4.9	nd	nd	4.360	5.306	13.8	0.11	27
◆	$27CZ_f$	25.6	3.8	18.4	nd	4.363	5.353	7.1	0.08	29
□	$1CZ/15CNF_f$	31.9	nd	20.9	nd	4.357	nd	11.8	0.14	40

XRD: X-ray diffraction patterns; BET: Brunauer–Emmet–Teller; nd: not detected; CZ: ceria–zirconia; CNF: carbon nanofibers.

presence of other peaks. Not all the crystallites are present as a mixed oxide, some segregations may have occurred.

XRD results are summarized in Table 2. The crystallite size of SiC varies from 27 to 31 nm. The size of ceria–zirconia particles are of 6.6 nm for the powder catalyst and 3.8 nm for the ceria–zirconia deposited on the SiC foam. The nickel particles are of 25 and 33 nm, respectively for SiC'_p and CZ_p. In the case of SiC_f, $15CNF_f$ and $1CZ_f$, the sizes of nickel particles are similar: 18–19 nm. The lattice parameters of SiC crystallites are also similar and vary between 4.35 and 4.36 Å. In the case of the ceria–zirconia catalysts, the lattice parameter of the powder and the foam catalyst are respectively of 5.268 and 5.353. The higher value of the second one is due to the presence of the segregated phases observed on the powder diffractogram.

The BET results are summarized in Table 2. The SiC powder catalyst, SiC'_p, has a specific surface area of $6\ m^2\ g^{-1}$, which is the lowest value observed. The SSA value of CZ_p is much higher: $31\ m^2\ g^{-1}$. The coating of foams with ceria–zirconia slightly increases their surface area from $25\ m^2\ g^{-1}$ to 27 and $29\ m^2\ g^{-1}$ respectively for $1CZ_f$ and $27CZ_f$. The foams covered with CNF have the highest surface area values: $40\ m^2\ g^{-1}$. The pore size of the SiC is of 18 and 15 nm respectively for the powder and foam catalyst. The pore size decreases when covered by nanofibers. This phenomenon is even more important for the foam coated with ceria–zirconia, with pore sizes of 14 and 7 nm for $1CZ_f$ and $27CZ_f$. The pore size seems to get closer to the value of powder ceria–zirconia: 4.4 nm. The pore volume values seem to be slightly higher when the foam is covered with carbon nanofibers, whereas those value decrease when the quantity of ceria–zirconia washcoat increases, the latter being due to the low pore volume values of ceria–zirconia synthesized by the pseudo sol-gel method.

The H_2-TPR results of the powder catalysts and of their corresponding supports are shown in Fig. 3 and summarized in Table 3. The reducibility of ceria–zirconia before impregnation is of 79% and of 76% after impregnation, assuming that all the Ni + Ru present is reduced into Ni^0 and Ru^0. One reduction peak at 360 °C can be attributed to the reduction of surface Ce^{3+} into Ce^{4+} according to the literature [37]. The peak at 381 °C can be attributed to the reduction of NiO particle of weak interaction with the ceria–zirconia support and the peak at 505 °C to the reduction of NiO particle of strong interaction with the ceria–zirconia support [38,39]. Another set of peaks is present between 164 °C and 220 °C. It is probably part of NiO and Ce^{3+} that is reduced at lower temperature due to their interaction with ruthenium particles, which renders their reduction easier. H_2-TPR of SiC powder shows practically no H_2 consumption, whereas for the reduction of the SiC'_p catalyst, hydrogen consumption is nearly twice the amount needed to reduce all the NiO and RuO_2 present. This higher consumption can be explained by a hydrogen spillover effect from the Ni + Ru metallic site to the SiO_2-SiO_xC_y sites of the washcoat [40]. In order to reduce most of the NiO and RuO_2 particles, a reduction at 400 °C of the catalyst is needed. Therefore, for the reactions made in the PMR, the foam will be reduced *ex situ* first, in a quartz tubular reactor, and afterwards a second reduction step at 220 °C inside the PMR to reduce the possible NiO layer formed on the metallic particles during the transfer of the foam from the tubular reactor into the PMR.

SEM micrographs of the foams of $27CZ_f$ (Fig. 4), $15CNF_f$ and $1CZ/15CNF_f$ (Fig. 5) were taken before impregnation with Ni + Ru. Fig. 4a and Fig. 5a clearly show that the struts

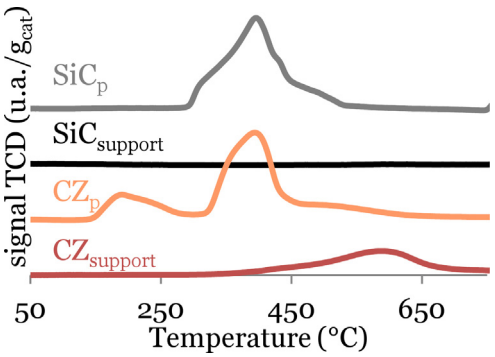

Fig. 3. (Color online.) Hydrogen temperature-programmed reduction (H_2-TPR) of the powder catalysts studied and their corresponding supports.

Table 3
Hydrogen consumption measured by H_2-TPD on the powder catalysts and their corresponding supports.

Catalyst	H_2 consumption (mmol/g)	H_2 theoretical consumption by Ni + Ru (mmol/g)	Ce^{3+}/Ce_{tot} after TPR
$CZ_{support}$	1.33	–	0.79
CZ_p	2.87	1.51	0.76
$SiC_{support}$	0.04	–	–
SiC'_p	2.81	1.72	–

H_2-TPR: hydrogen temperature programmed reduction; CZ: ceria–zirconia.

have a triangular shape and are hollow, which is distinctive for foams synthesized with the shape memory synthesis method described by Pham-Huu et al. [41]. Fig. 4a and b show that the whole surface of the foam is coated with CZ. The thickness of the coating was measured using Fig. 4c, giving an average thickness of 27 μm.

Fig. 5a and b show that the foams with CNF are entirely covered with a dense network of carbon nanofibers, without closing cells or windows. The CNF diameters are between 20 and 50 nm, which is usually observed for carbon nanofibers grown over nickel particles using ethane [42]. In the case of foams with carbon nanofibers coated with ceria–zirconia, it can be observed in Fig. 5c that part of ceria–zirconia forms aggregates on the surface of the foam. However the nanofibers diameter measured using Fig. 5d are now between 30 and 80 nm, which clearly indicates that there is a washcoat of ceria–zirconia over the CNF.

3.2. Catalytic test

A study of the catalytic activity as a function of the temperature was made for all the catalysts mentioned previously and the results of CO_2 conversion rates and productivity are displayed in Figs. 6 and 7. For each test, the

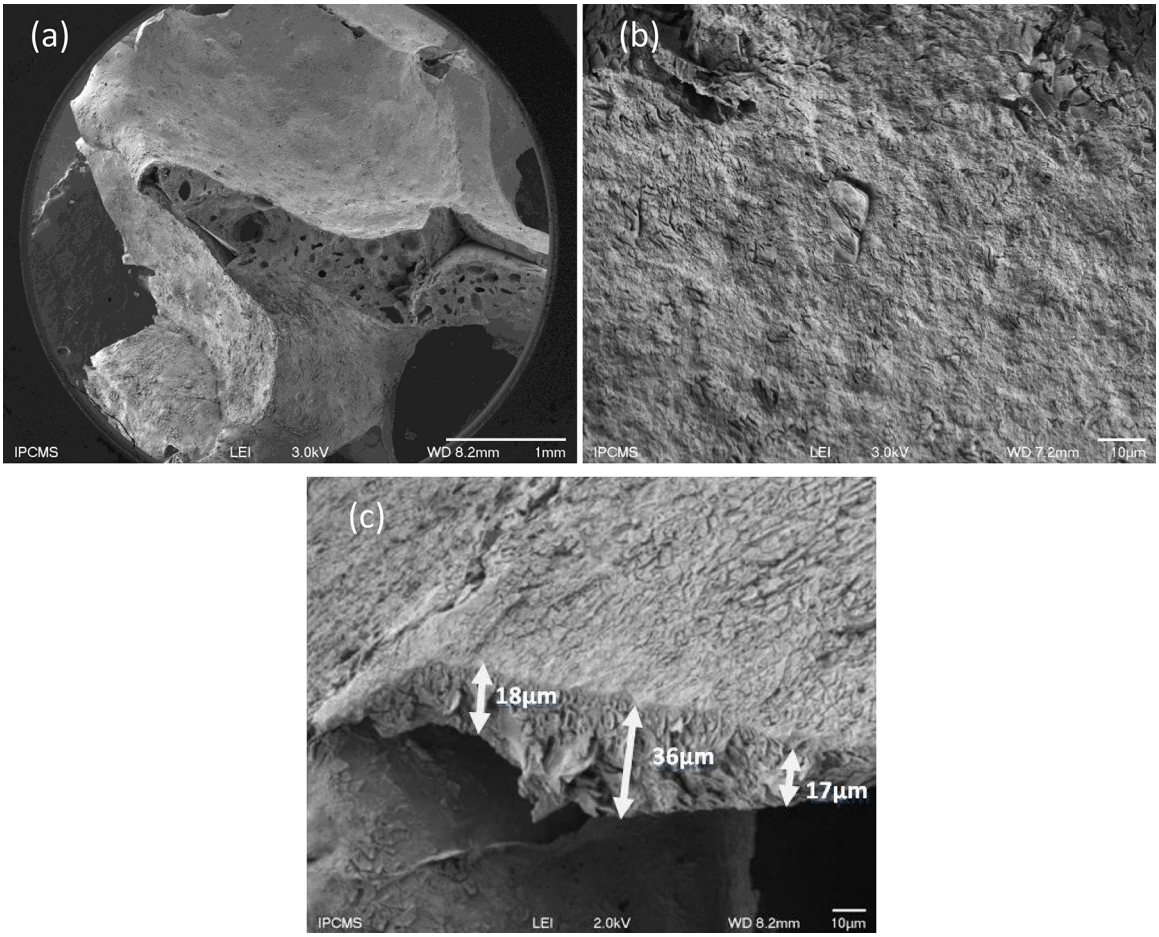

Fig. 4. Scanning electron microscopy (SEM) micrographs of 27 ceria–zirconia $(CZ)_f$ before impregnation with Ni + Ru.

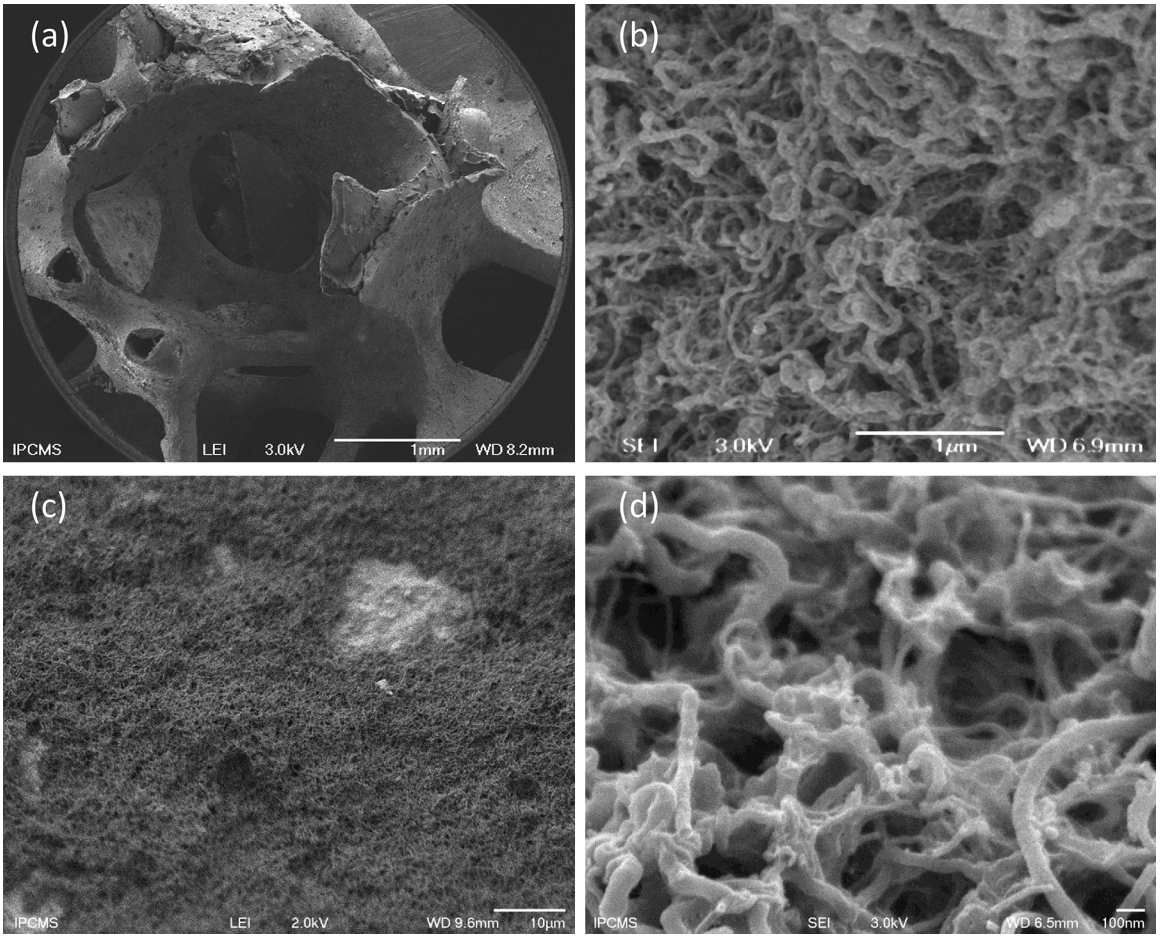

Fig. 5. Scanning electron microscopy (SEM) micrographs: a and b: foam 15 carbon nanofibers $(CNF)F_f$; c and d: ceria–zirconia (CZ)/$15CNF_f$ (both before impregnation with Ni + Ru).

mass of Ni + Ru involved (depending on the catalyst density and composition) as well as the methane selectivities and side products at 250, 300 and 400 °C are presented in Table 4.

Regarding the powder catalysts studied (Fig. 6), the CO_2 conversion rates and methane selectivity at 250 °C are of 35.5% and 98.3% for CZ_p while SiC'$_p$ those values are of 5.0% and 94%. The same trend is observed for higher temperatures. The ceria–zirconia-based catalyst is better than SiC.

The differences between foam and powder catalysts have been investigated, comparing SiC catalysts, SiC'$_p$ and SiC'$_f$, and ceria–zirconia-based catalysts, $27CZ_f$ and CZ_p diluted with SiC powder giving a 30-70 CZ_p–SiC_p ratio in order to have the same chemical composition as that of

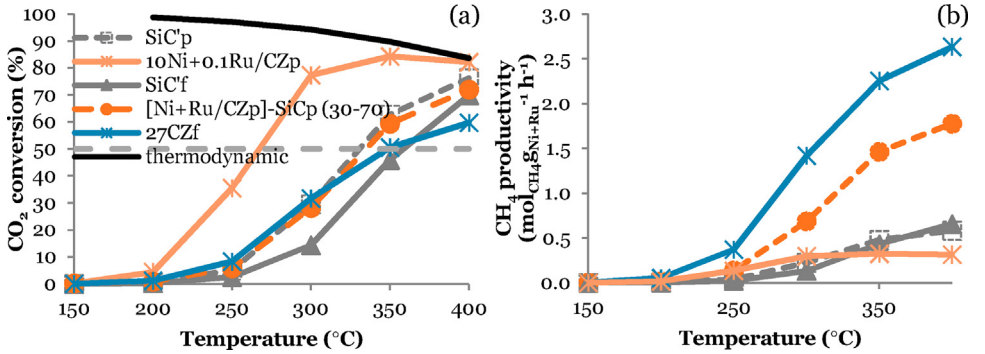

Fig. 6. (Color online.) a: CO_2 conversion values of the powder catalysts and their corresponding foam catalysts studied at Gas Hourly Space Velocity (GHSV) 10,000·h^{-1} and thermodynamic values calculated for CO_2 conversion at various temperatures; b: CH_4 productivity values of the catalysts studied at GHSV 10,000·h^{-1} for various temperatures.

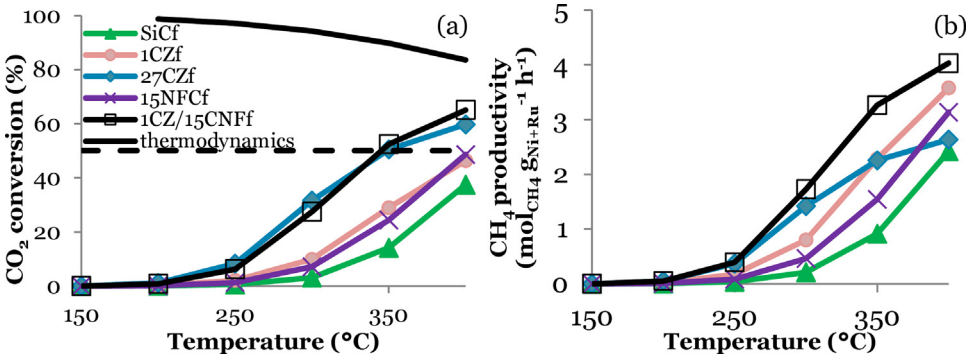

Fig. 7. (Color online.) a: CO_2 conversion values of the foam catalysts studied at GHSV 10,000·h^{-1} and thermodynamic values calculated for CO_2 conversion at various temperatures; b: CH_4 productivity values of the catalysts studied at Gas Hourly Space Velocity (GHSV) 10,000·h^{-1} for various temperatures.

$27CZ_f$ (72.5 wt% SiC, 27 wt% CZ, 2.5 wt% Ni and 0.025 wt% Ru). The results are presented in Fig. 6 and in Table 4. At 250 °C, the CO_2 conversion values of SiC'_p and SiC'_f are respectively of 5.0% and 2.5%. The same trend can be observed at higher temperatures: for similar compositions, the powder catalyst is always more active than the foam catalyst. For the ceria–zirconia-based catalysts, the powder (CZ_p–SiC_p) and foam catalysts ($27CZ_f$) have respectively CO_2 conversion values of 5.8 and 8.3% at 250 °C. For higher temperatures (400 °C), the powder catalyst shows higher CO_2 conversion rates with values of 72.0% against 59.8% for $27CZ_f$.

The foam catalysts seem to have lower conversion rates, but in order to compare powder and foam catalysts, the parameter kept unchanged is the apparent volume of the catalytic bed. Therefore, the catalyst loading is less important due to the lower density of foams compared to powders. Consequently, a better comparison between foam and powder can be made if the productivity results are considered (Fig. 6 and Table 4). In the case of SiC'_p and SiC'_f, both curves are superimposed. The ceria–zirconia-based foam ($27CZ_f$) has productivity values that range from 0.37 to 2.63 $mol_{CH_4}\cdot g_{Ni+Ru}{}^{-1}\cdot h^{-1}$ between 250 °C and 400 °C against 0.1 to 1.8 $mol_{CH_4}\cdot g_{Ni+Ru}{}^{-1}\cdot h^{-1}$ for the CZ/SiC mixture. Finally, at

Table 4
(Color online.) CO_2 conversion, methane, CO and ethane selectivities and productivity values at 250 °C, 300 °C and 400 °C at GHSV 10,000·h^{-1}.

Catalyst		m_{Ni+Ru} (mg)	Temperature (°C)	X_{CO2}	S_{CH4}	S_{CO}	S_{C2H6}	P_{CH4}
⬚	SiC'_p	14.4	250	5.0	94.0	4.7	0.4	0.04
			300	29.6	93.9	6.0	0.0	0.21
			400	76.2	98.4	1.4	0.0	0.57
✖	CZ_p	28.5	250	35.5	98.3	0.4	1.0	0.13
			300	77.3	99.5	0.3	0.2	0.30
			400	82.2	99.3	0.8	0.0	0.31
●	SiC_p–CZ_p (70-30)	4.4	250	5.8	93.5	3.1	1.5	0.1
			300	28.2	96.8	2.3	0.9	0.7
			400	72.0	98.0	1.9	0.1	1.8
△	SiC'_f	11.7	250	2.5	87.2	12.5	0.0	0.02
			300	14.3	87.7	12.2	0.0	0.12
			400	69.9	93.9	4.3	0.0	0.62
▲	SiC_f	1.3	250	0.6	74.5	23.3	0.0	0.04
			300	3.2	79.3	20.7	0.0	0.21
			400	37.5	76.6	23.1	0.0	2.42
×	$15CNF_f$	1.5	250	1.3	88.1	13.3	0.0	0.09
			300	7.1	87.3	12.7	0.0	0.46
			400	48.6	86.5	12.7	0.0	3.13
+	$1CZ_f$	1.3	250	2.1	99.3	2.8	0.7	0.18
			300	9.9	97.1	2.6	0.3	0.80
			400	46.4	92.3	8.3	0.0	3.58
◆	$27CZ_f$	2.4	250	8.3	97.5	2.1	0.5	0.37
			300	31.6	98.1	1.7	0.2	1.42
			400	59.8	96.4	3.9	0.0	2.63
□	$1CZ/15CNF_f$	1.7	250	6.3	97.7	1.9	0.4	0.39
			300	27.5	97.7	3.1	0.2	1.73
			400	65.1	96.2	3.8	0.0	4.03

GHSV: Gas Hourly Space Velocity; CZ: ceria–zirconia; CNF: carbon nanofibers.

250 °C, the methane selectivities of SiC'$_p$ and SiC'$_f$ are respectively of 94.0% and 87.2%, while the CO selectivities are of 4.7% and 12.5%. In the case of ceria–zirconia, at 250 °C, the foam catalyst has respectively methane and CO selectivities of 97.5% and 2.1%, and the SiC/CZ mixture 93.5% and 3.1%.

To conclude, the productivities of SiC'$_p$ and SiC'$_f$ are similar, while the CO selectivities are higher for the foam catalyst SiC'$_f$. In the case of ceria-based-catalysts, 27CZ$_f$ clearly shows the best productivity values and higher methane selectivities than the powder catalyst (CZ$_p$–SiC$_p$).

Fig. 7 and Table 4 allow us to compare the influence of ceria–zirconia, carbon nanofibers and carbon nanofibers combined with ceria–zirconia washcoats on the carbon dioxide methanation reaction. The conversion values of SiC$_f$ (Fig. 7a), 15CNF$_f$, 1CZ$_f$ and 27CZ$_f$ at 250 °C are respectively of 0.6%, 1.3%, 2.1% and 8.3% and their productivity values (Fig. 7b) from 250 °C to 300 °C are 0.04–0.21, 0.09–0.46, 0.18–0.80, and 0.39–1.42 $mol_{CH4}{\cdot}g_{Ni+Ru}{}^{-1}{\cdot}h^{-1}$. The presence of carbon nanofibers has a positive effect on the catalyst's activity and ceria–zirconia seems to have a higher effect on the conversion rates. Moreover, the methane selectivities of SiC$_f$, 1CZ$_f$, 27CZ$_f$ and 15CNF$_f$ are respectively of 75–79%, 92–99%, 96–98% and 87–88%. Catalyst SiC$_f$ has the lowest methane productivity and CO_2 conversion rates and more than 20% of selectivity for CO, which is too high to consider a direct injection of these reaction products into the natural gas transmission network. The CO_2 conversion rates of 15CNF$_f$ are higher than for SiC$_f$, but the average CO selectivity of 13% is still too high. Still, those results show the beneficial effect of the carbon nanofibers on the catalytic activity by increasing the conversion rates and lowering the selectivity for CO. The CO_2 conversion values of 27CZ$_f$ are higher and its productivity better due to the higher selectivity in methane and consequently lower CO selectivity (2–4%). Decreasing the ceria–zirconia loading to 1 wt% (1CZ$_f$) shows similar conversion values than for 15CNF$_f$, but higher methane productivities and selectivities than for 15CNF$_f$.

Catalyst 1CZ/15CNF$_f$ was prepared to see if a combined effect of ceria–zirconia and carbon nanofibers could be achieved. For this catalysts, the CO_2 conversion rates are of 6.3% at 250 °C, which is close to the values of 27CZ$_f$ (8.3%), and the methane selectivities of 96–98% are the same as for 27CZ$_f$. However, the productivity values of 0.39–1.73 $mol_{CH4}{\cdot}g_{Ni+Ru}{}^{-1}{\cdot}h^{-1}$ ranging from 250 °C to 300 °C are higher for 1CZ/15CNF$_f$ than 27CZ$_f$ ($0.18-0.80\ mol_{CH_4}{\cdot}\,g_{Ni+Ru}{}^{-1}{\cdot}\,h^{-1}$). The comparison of 1CZ/15CNF$_f$ and 1CZ$_f$, which both have the same ceria–zirconia loading, shows that the CO_2 conversion rate, which is of 2.1% and 6.3% at 250 °C for 1CZ/15CNF$_f$ and 1CZ$_f$, respectively, is higher for 1CZ/15CNF$_f$. Moreover, the same trend is observed for productivity values of 0.39–4.03 and $0.18-3.58\ mol_{CH_4}{\cdot}\,g_{Ni+Ru}{}^{-1}{\cdot}\,h^{-1}$ for 1CZ/15CNF$_f$ and 1CZ, respectively.

Consequently, the catalyst that will be used for the heat transfer study through infrared imaging is 1CZ/15CNF$_f$.

The conversion rate of the chosen catalyst at 250 °C is of 6.3%. This value seems low, but the catalytic tests were performed in a quartz tubular reactor with a bed apparent volume of 0.15 cm^3 and a flow rate of 1.5 $L{\cdot}h^{-1}$ in order to have a GHSV of 10,000$\cdot h^{-1}$, high enough to allow a better comparison of the catalyst without being limited by the thermodynamic equilibrium. The bed volume in the PMR will be of 1.1 cm^3, the flow rates will vary from 2 to 5 $L{\cdot}h^{-1}$; consequently the GHSV will be lowered between 1800 to 4600 h^{-1}. Therefore, the residence time will be much higher and the catalyst activity will be higher; the conversion rates at 250 °C are thus expected to be higher than 6%.

4. Conclusion

The objective of this work was to develop a catalyst with enough catalytic activity at temperatures below 250 °C (CO_2 conversion rate of 10–20%) in order to study the heat transfer in a PMR filled with cellular foam using an infrared camera.

The specific surface area of the commercial SiC foam was successfully increased either by coating the foam with ceria–zirconia or by growing carbon nanofibers on the foam. The beneficial effect on the catalytic activity of ceria–zirconia and carbon nanofibers on the SiC foam was also revealed. Furthermore, the ceria–zirconia catalysts showed higher conversion rates and the presence of ceria–zirconia was proven to be necessary in order to have the lowest CO selectivity values and therefore the highest methane productivity. Finally, combining the positive effect of ceria–zirconia and carbon nanofibers gave the best productivity results and therefore, the catalyst 1CZ/15CNF$_f$ was chosen for the heat transfer study.

Acknowledgments

The authors would like to thank the ANR (ANR2010JCJC90401 SIMI9 'Millimatrix) and the Région Alsace for their financial support.

References

[1] F. Lecomte, P. Broutin, E. Lebas, Le captage du CO_2 : des technologies pour réduire les émissions à effet de serre, Technip, Paris, 2009.
[2] J. Wambach, A. Baiker, A. Wokaun, Phys. Chem. Chem. Phys. 1 (1999) 5071.
[3] https://www.enertrag.com/fr/developpement-de-projet/la-centrale-hybride.html, 27/06/2014.
[4] E. Meza, Audi opens 6MW power-to-gas facility,http://www.pv-magazine.com/news/details/beitrag/audi-opens-6-mw-power-to-gas-facility_100011859/.
[5] P. Sabatier, J.-B. Senderens, C. R. Acad. Sci. Paris 134 (1978) 514.
[6] P. Sabatier, J.-B. Senderens, C. R. Acad. Sci. Paris 134 (1902) 689.
[7] W. Makowski, R. Dziembaj, J. Mol. Catal. 91 (1994) 353.
[8] A. Beuls, C. Swalus, M. Jacquemin, G. Heyen, A. Karelovic, P. Ruiza, Appl. Catal., B Environ. 113–114 (2012) 2.
[9] F. Ocampo, B. Louis, L. Kiwi-Minsker, A.-C. Roger, Appl. Catal., A Gen. 392 (2011) 36.
[10] S. Sharma, Z. Hu, P. Zhang, E.W. McFarland, H. Metiu, J. Catal. 278 (2011) 297.
[11] S. Fujita, N. Takezawa, Chem. Eng. J. 68 (1997) 63.
[12] Y. Zhang, G. Jacobs, D.E. Sparks, M.E. Dry, B.H. Davis, Catal. Today 71 (2002) 411.
[13] H. Song, J. Yang, J. Zhao, L. Chou, Chinese J. Catal. 31 (2010) 21 (Chinese version).
[14] C. Bartholomew, J. Catal. 65 (1980) 390.
[15] A.E. Aksoylu, Z. Misirli, Z.I. Önsan, Appl. Catal., A Gen. 168 (1998) 385.
[16] S. Tada, T. Shimizu, H. Kameyama, T. Haneda, R. Kikuchi, Int. J. Hydrogen Energy 37 (2012) 5527.
[17] M. Cai, J. Wen, W. Chu, X. Cheng, Z. Li, J. Nat. Gas Chem. 20 (2011) 318.

[18] G. Zhi, X. Guo, Y. Wang, G. Jin, X. Guo, Catal. Commun. 16 (2011) 56.
[19] F.-W. Chang, M.-S. Kuo, M.-T. Tsay, M.-C. Hsieh, Appl. Catal., A Gen. 247 (2003) 309.
[20] H. Takano, K. Izumiya, N. Kumagai, K. Hashimoto, Appl. Surf. Sci. 257 (2011) 8171.
[21] F. Ocampo, B. Louis, A.-C. Roger, Appl. Catal., A Gen. 369 (2009) 90.
[22] K.P. Jackel, Microsystem Technology for Chemical and Biological Microreactors, in: Papers of the Workshop on Microsystem Technology, Mainz, 20–21 February, 1995: Organized by Dechema and Imm, Dechema, 1996.
[23] M.W. Losey, M.A. Schmidt, K.F. Jensen, Ind. Eng. Chem. Res. 40 (2001) 2555.
[24] O. Wörz, K.-P. Jäckel, T. Richter, A. Wolf, Chem. Eng. Technol. 24 (2001) 138.
[25] http://www.sicatcatalyst.com/.
[26] J.-M. Ledoux, J.-L. Guille, S. Hantzer, D. Dubots, Process for the Production of Silicon Carbide with a Large Specific Surface Area and Use for High Temperature Catalytic Reactions, Patent No. US4914070 A, 1990.
[27] D. Édouard, S. Ivanova, M. Lacroix, E. Vanhaecke, C. Pham, C. Pham-Huu, Catal. Today 141 (2009) 403.
[28] S. Ivanova, E. Vanhaecke, S. Libs, B. Louis, C. Pham-Huu, M. Ledoux, Déshydratation du methanol en diméthyléther employant des catalyseurs a base d'une zeolithe supportee sur du carbure de silicium, Patent No. PCT/FR2007/002017, 2008.
[29] Y. Liu, S. Podila, D.L. Nguyen, D. Édouard, P. Nguyen, C. Pham, M.J. Ledoux, C. Pham-Huu, Appl. Catal., A Gen. 409–410 (2011) 113.
[30] T.T. Nguyen, L. Burel, D.L. Nguyen, C. Pham-Huu, J.M.M. Millet, Appl. Catal., A Gen. 433–434 (2012) 41.
[31] Y. Liu, D. Édouard, L.D. Nguyen, D. Begin, P. Nguyen, C. Pham, C. Pham-Huu, Chem. Eng. J. 222 (2013) 265.
[32] P.A.U. Aldana, F. Ocampo, K. Kobl, B. Louis, F. Thibault-Starzyk, M. Daturi, P. Bazin, S. Thomas, A.C. Roger, Catal. Today 215 (2013) 201.
[33] F. Ocampo, Développement de catalyseurs pour la réaction de méthanation du dioxyde de carbone, (PhD Thesis), Université de Strasbourg, France, 2011.
[34] H.P. Klug, L.E. Alexander, X-Ray Diffraction Procedures, John Wiley and Sons, New York, 1956.
[35] A.E. Nelson, K.H. Schulz, Appl. Surf. Sci. 210 (2003) 206.
[36] A. Kozlov, J. Catal. 209 (2002) 417.
[37] H. Yao, J. Catal. 86 (1984) 254.
[38] A.M. Diskin, R.H. Cunningham, R.M. Ormerod, Catal. Today 46 (1998) 147.
[39] M.A. Małecka, L. Kępiński, W. Mišta, J. Alloys Compd. 451 (2008) 567.
[40] W.C. Conner, J.L. Falconer, Chem. Rev. 95 (1995) 759.
[41] C. Pham-Huu, N. Keller, G. Ehret, M.J. Ledoux, J. Catal. 200 (2001) 400.
[42] N.A. Jarrah, J.G. van Ommen, L. Lefferts, J. Mater. Chem. 14 (2004) 1590.